The Astrophysical Journal, 825:151 (5pp), 2016 July 10 doi:10.3847/0004-637X/825/2/151

A CANDIDATE OPTICAL COUNTERPART TO THE MIDDLE AGED γ-RAY PULSAR PSR J1741–2054*

R. P. Mignani[1,2], V. Testa[3], M. Marelli[1], A. De Luca[1,4], D. Salvetti[1], A. Belfiore[1], M. Pierbattista[5], M. Razzano[6], A. Shearer[7], and P. Moran[7]

[1] INAF—Istituto di Astrofisica Spaziale e Fisica Cosmica Milano, via E. Bassini 15, I-20133, Milano, Italy
[2] Janusz Gil Institute of Astronomy, University of Zielona Góra, Lubuska 2, 65-265, Zielona Góra, Poland
[3] INAF—Osservatorio Astronomico di Roma, via Frascati 33, I-00040, Monteporzio, Italy
[4] Istituto Nazionale di Fisica Nucleare, Sezione di Pavia, Via Bassi 6, I-27100 Pavia, Italy
[5] Department of Astrophysics and Theory of Gravity, Maria Curie-Sklodowska University, ul. Radziszewskiego 10, 20-031 Lublin, Poland
[6] Istituto Nazionale di Fisica Nucleare, Sezione di Pisa, I-56127 Pisa, Italy
[7] Centre for Astronomy, National University of Ireland, Newcastle Road, Galway, Ireland
Received 2016 April 7; revised 2016 May 2; accepted 2016 May 6; published 2016 July 13

ABSTRACT

We carried out deep optical observations of the middle aged γ-ray pulsar PSR J1741−2054 with the Very Large Telescope (VLT). We identified two objects, of magnitudes $m_v = 23.10 \pm 0.05$ and $m_v = 25.32 \pm 0.08$, at positions consistent with the very accurate *Chandra* coordinates of the pulsar, the faintest of which is more likely to be its counterpart. From the VLT images we also detected the known bow-shock nebula around PSR J1741 −2054. The nebula is displaced by ∼0.″9 (at the 3σ confidence level) with respect to its position measured in archival data, showing that the shock propagates in the interstellar medium consistently with the pulsar proper motion. Finally, we could not find evidence of large-scale extended optical emission associated with the pulsar wind nebula detected by *Chandra*, down to a surface brightness limit of ∼28.1 mag arcsec^{-2}. Future observations are needed to confirm the optical identification of PSR J1741−2054 and characterize the spectrum of its counterpart.

Key words: pulsars: individual (PSRJ1741–2054)

1. INTRODUCTION

PSR J1741−2054 in the Ophiuchus constellation is one of the first γ-ray pulsars to have been discovered by the Large Area Telescope (LAT; Atwood et al. 2009) on board the *Fermi Gamma-ray Space Telescope* through a blind search for pulsations (Abdo et al. 2009). Its spin period ($P_s = 413$ ms) and its derivative ($\dot{P}_s = 1.698 \times 10^{-14}$ s s^{-1}) yield a characteristic age $\tau = 0.386$ Myr. The spin parameters also yield a rotational energy-loss rate $\dot{E}_{rot} = 9.5 \times 10^{33}$ erg s^{-1} and a dipolar surface magnetic field $B_s = 2.68 \times 10^{12}$ G. Soon after its γ-ray detection, PSR J1741−2054 was also discovered as a radio pulsar in archival data from the Parkes telescope. Observations with the Green Bank Telescope yielded a dispersion measure (DM) of 4.7 pc cm^{-3} (Camilo et al. 2009) which, from the NE2001 model of the Galactic free electron density (Cordes & Lazio 2002), corresponds to a distance of ∼0.38 kpc. Its very faint radio flux (∼0.16 mJy at 1.4 GHz; Camilo et al. 2009) and small distance make PSR J1741−2054 the least luminous radio pulsar. PSR J1741−2054 is also one of the very few middle aged ($\tau \sim 0.1$–1 Myr) γ-ray pulsars closer than ∼0.5 kpc (see Abdo et al. 2013).

The X-ray counterpart to PSR J1741−2054 was found by *Swift* (Camilo et al. 2009) soon after its detection as a radio pulsar. The X-ray identification was confirmed by *Chandra* observations that also detected a compact pulsar wind nebula (PWN) around PSR J1741−2054 and an ∼1.′5 long trail of X-ray emission (Romani et al. 2010). The pulsar was also observed with *XMM-Newton* (Marelli et al. 2014) and X-ray pulsations were detected for the first time. Its X-ray spectrum is characterized by the combination of a power law (PL) and a blackbody (BB), like in other middle aged pulsars, produced by emission from the neutron star magnetosphere and the cooling neutron star surface. An analysis of the *Chandra* data was done by Karpova et al. (2014) and Auchettl et al. (2015), who also measured the pulsar proper motion ($\mu = 109 \pm 10$ mas yr^{-1}) from the analysis of multi-epoch observations. The proper motion corresponds to a transverse velocity of 196 ± 18 km s^{-1} for a pulsar distance of 0.38 kpc.

The close distance to PSR J1741−2054 makes it a promising target for a detection in the optical band. Indeed, the middle aged γ-ray pulsars PSR B0656+14, Geminga, and PSR B1055 −52 have all been identified in the optical (Abdo et al. 2013 and references therein) due to their distances, closer than ∼0.5 kpc. Observations of the PSR J1741−2054 field in the H_α band (Romani et al. 2010; Brownsberger & Romani 2014) allowed us to discover a bow-shock nebula, produced by the pulsar motion in the interstellar medium (ISM), whose axis of symmetry is aligned with the major axis of the PWN trail and with the direction of the pulsar proper motion (Auchettl et al. 2015). The pulsar, however, remained undetected at optical wavelengths. Interestingly, optical spectroscopy of the bow-shock nebula (Romani et al. 2010) yielded a pulsar space velocity consistent with that inferred from its proper motion and a DM distance of 0.38 kpc, suggesting that this value is qualitatively correct.

Here, we present the analysis of deep optical observations of PSR J1741−2054 carried out with the ESO Very Large Telescope (VLT). Observations and data analysis are described in Section 2, while the results are presented and discussed in Sections 3 and 4, respectively.

2. OBSERVATIONS AND DATA REDUCTION

PSR J1741−2054 was observed in service mode on 2015 May 14 and 15 with the VLT at the ESO Paranal Observatory

* Based on observations collected at the European Organization for Astronomical Research in the Southern Hemisphere under ESO programme 095.D-0328(B).

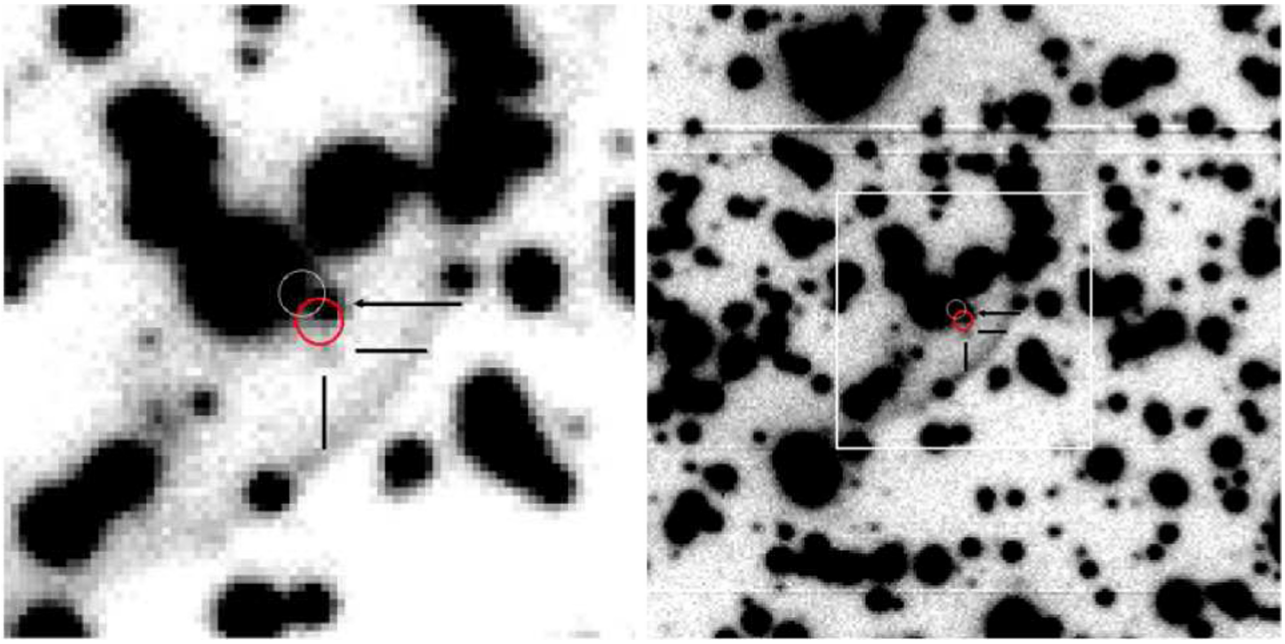

Figure 1. Left: FORS2 image ($10'' \times 10''$) of the PSR J1741−2054 field (b_{HIGH} filter). North is to the top, and east is to the left. The circles ($0\farcs36$ radii, accounting for our astrometry accuracy) mark the reference pulsar position (Romani et al. 2010; MJD 55337; white) and that corrected for the proper motion (Auchettl et al. 2015) at the VLT epoch (MJD 57156; red). Two objects, marked by the arrow and the two ticks, are visible near it. Right: Wider zoom ($25'' \times 25''$) of the same area with the image contrast adjusted to better show the arc-like structure south and west of the pulsar.

and the second FOcal Reducer and low dispersion Spectrograph (FORS2; Appenzeller et al. 1998) in imaging mode. The camera was equipped with its default MIT detector, a mosaic of two 4 k × 2 k CCDs aligned along the long axis, optimized for wavelengths longer than 6000 Å. With the FORS2 high-resolution collimator, the detector has a pixel scale of $0\farcs125$ (2 × 2 binning) and a projected field-of-view of $4\farcm15 \times 4\farcm15$. The observations were executed with the standard low-gain and fast read-out mode and through the high-throughput b_{HIGH} ($\lambda = 4400$ Å; $\Delta\lambda = 1035$ Å) and v_{HIGH} ($\lambda = 5570$ Å; $\Delta\lambda = 1235$ Å) filters. To allow for cosmic-ray removal and reduce the impact of bright star saturation, we obtained sequences of 30 short exposures (180 s) for a total integration time of 5400 s in both the b_{HIGH} and v_{HIGH} filters. Exposures were taken in dark time and under clear sky conditions, with the target close to the zenith (airmass $\lesssim$1.1) and seeing $\sim0\farcs4$.

We reduced the data (bias subtraction and flat–fielding) using tools in the IRAF[8] package CCDRED. Per each band, we aligned and average-stacked the reduced science images with the `drizzle` task in IRAF, applying a σ clipping to filter out hot/cold pixels and cosmic-ray hits. We applied the photometric calibration by using the FORS2 night zero points and the atmospheric extinction coefficients.[9] We computed the astrometry calibration using the *wcstools*[10] suite of programs and reference stars from the GSC2.3 (Lasker et al. 2008). We obtained mean residuals of $\lesssim0\farcs1$ in the radial direction, using 30 non-saturated GSC2.3 stars selected to avoid the vignetted regions of the detector. Due to the pixel scale of the FORS2 images ($0\farcs125$), the uncertainty on the centroids of the reference stars is negligible. To this value we added in quadrature the uncertainty of the image registration on the GSC-2.3 reference frame ($\sim0\farcs11$) and the $0\farcs15$ uncertainty on the link of the GSC2.3 to the International Celestial Reference Frame. We ended up with an overall accuracy of $\sim0\farcs2$ on our absolute astrometry.

3. RESULTS

As a reference to search for the PSR J1741−2054 optical counterpart, we used its *Chandra* coordinates $\alpha = 17^{h}41^{m}57\overset{s}{.}28$; $\delta = -20°54'11\farcs8$ (MJD 55337), with an estimated accuracy of $0\farcs3$ (Romani et al. 2010). We note that SIMBAD currently reports the pulsar γ-ray coordinates from the Third *Fermi*-LAT γ-ray source catalog (Acero et al. 2015), whereas those in the ATNF pulsar database (Manchester et al. 2005) are inconsistent with the published ones (Camilo et al. 2009; Romani et al. 2010). We accounted for the *Chandra* proper motion[11] $\mu_\alpha \cos(\delta) = -63 \pm 12$ mas yr^{-1} and $\mu_\delta = -89 \pm 9$ mas yr^{-1} (Auchettl et al. 2015) to extrapolate the pulsar coordinates at the epoch of our VLT observations (MJD 57156). The error on the proper motion produces an uncertainty on the coordinate extrapolation ($\sim0\farcs06$) negligible compared to that of the reference *Chandra* coordinates and the accuracy of our astrometry calibration.

A close up view of the FORS2 b_{HIGH}-band image centered on the extrapolated PSR J1741−2054 position is shown in Figure 1 (left). An object is clearly detected within the position error circle of magnitudes $m_b = 24.76 \pm 0.07$ and $m_v = 23.10 \pm 0.05$. A second fainter object ($m_b = 26.45 \pm 0.10$ and $m_v = 25.32 \pm 0.08$) is visible south of it within $\sim1.5\sigma$ from the expected pulsar position. To minimize the effects of the bright

[8] IRAF is distributed by the National Optical Astronomy Observatories, which are operated by the Association of Universities for Research in Astronomy, Inc., under cooperative agreement with the National Science Foundation.

[9] www.eso.org/observing/dfo/quality/FORS2/qc/qc1.html

[10] http://tdc-www.harvard.edu/wcstools

[11] Note that μ_δ is reported with the wrong sign on page 70 of Auchettl et al. (2015).

stars north of the pulsar position, we computed the objects magnitudes through point-spread function (PSF) photometry with the DAOPHOT II package (Stetson 1994) in IRAF and applied the aperture correction. Owing to its position close to the Galactic plane ($l = 6.^\circ4$; $b = 4.^\circ9$), the field of PSR J1741−2054 is very crowded. Therefore, we cannot rule out the possibility of a chance coincidence with the proper-motion-corrected *Chandra* position. Assuming a Poisson distribution, the probability of a having at least a spurious association within a given matching radius is $P = 1 - \exp(-\lambda)$, where $\lambda = \pi\rho\, r^2$, r is the association radius and ρ is the number density of field objects of brightness between that of the two objects and the image detection limit. For $\rho \sim 0.14$ arcsec^{-2}, as measured by the number of objects counted in the FORS2 images, and $r \sim 0.''46$, chosen as the angular separation between the center of the error circle and the southernmost of the two objects, we derived that $P \sim 0.09$. If PSR J1741−2054 had an optical luminosity of the same order of magnitude as PSR B0656+14, Geminga, and PSR B1055−52, which are at a similar distance, we would expect that its optical brightness be in the range $m_v \approx 25$–26. This would make the faintest of the two objects above a more likely candidate counterpart to the pulsar. Without further evidence, we cannot firmly rule out the other object as a candidate counterpart, though. In this case, however, PSR J1741−2054 would be about 10 times brighter than the other three middle aged pulsars, unless its distance is overestimated by a factor of three. Such a small distance would be incompatible with the significant hydrogen column density $N_{\rm H}$ in the pulsar direction (Marelli et al. 2014) and with the measurements of the pulsar space velocity (Romani et al. 2010; Auchettl et al. 2015), which are in agreement with the DM-based distance. Further observations will solve this possible ambiguity, e.g., by measuring for the candidate counterpart the same proper motion as the pulsar, which would secure its identification.

Figure 1 (right) shows a zoom out of the FORS2 image around the PSR J1741−2054 position. A region of extended emission with an arc-like structure is clearly visible around the pulsar, with a spatial extent and morphology very similar to those of the bow-shock nebula detected in H_α by Romani et al. (2010). The arc-like structure in Figure 1 is not seen in the $v_{\rm HIGH}$-band image. We identify this structure with the bow-shock nebula around the pulsar and attribute its origin to the contribution of the H_γ and H_β emission lines in the bow-shock spectrum (Romani et al. 2010). The wavelengths of these lines fall within the bandwidth of the $b_{\rm HIGH}$ filter but not of the $v_{\rm HIGH}$ one (see Section 2), which explains the non-detection of the structure in the latter filter.

We compared both the position and morphology of the bow-shock nebula with those observed in images taken back on 2009 August 21 (MJD = 55063) by Romani et al. (2010) with the ESO New Technology Telescope (NTT). The data set, retrieved from the public ESO archive, includes three exposures in H_α (600 s each) taken with the ESO Faint Object Spectrograph and Camera (EFOSC; Buzzoni et al. 1984), with a spatial resolution of $0.''25$/pixel. We reduced the data and applied the astrometry calibration as described in Section 2. Figure 2 (left) shows the NTT image with the contours of the VLT/FORS2 image overlaid. Although the morphology of the bow-shock nebula is consistent in the two images, its position in the VLT one is slightly offset to the southwest, i.e., close to the direction of the pulsar proper motion (position angle 215° ± 6°, measured east of north). We measured this displacement by comparing the relative positions of the peaks of the nebula surface brightness measured in a rectangle of $3.''5 \times 1.''6$ around its axis of symmetry and found that it amounts to $0.94^{+0.20}_{-0.31}$ arcsec. The timespan between the VLT and NTT images (∼5.7 years) implies an annual nebula displacement of 169^{+35}_{-54} mas yr^{-1}, consistent with the pulsar proper motion (109 ± 10 mas yr^{-1}). Therefore, the nebula displacement is explained by the shock propagation in the ISM as a result of the pulsar proper motion. We also note that for the northern rim of the nebula there is a hint of a larger displacement than for the southern one. This suggests a different propagation velocity of the shock along the north−south direction, probably due to a difference in the local density of the ISM. PSR J1741–2054 is thus only the third pulsar for which a displacement of the H_α bow-shock nebula has been detected after PSR B2224+65 with its renown "Guitar" nebula (Chatterjee & Cordes 2002), and PSR J0437−4715 (e.g., Brownsberger & Romani 2014).

On a much larger scale, we found no evidence of diffuse optical emission which can be associated with the X-ray PWN (Figure 2, right). From our broadband images, which cover the entire PWN area, we estimated 3σ upper limits of ∼27.8 and ∼28.1 mag arcsec^{-2} on its optical surface brightness in the $b_{\rm HIGH}$ and $v_{\rm HIGH}$ bands, respectively. These limits have been computed by averaging measurements obtained in a grid of star-free regions along the PWN.

4. DISCUSSION

Owing to their faintness, only 8 of the over 200 γ-ray pulsars discovered to date[12] have been detected at optical wavelengths (see Abdo et al. 2013 and references therein), the number also accounting for PSR B0540−69 (Caraveo et al. 1992), which was only recently found to be a γ-ray pulsar (Ackermann et al. 2015). Furthermore, candidate counterparts have been found for PSR J0205+6449 (Moran et al. 2013) and PSR J1357−6429 (Zyuzin et al. 2016). Here, we found a candidate counterpart to another γ-ray pulsar, PSR J1741−2054.

We compared its fluxes with the extrapolation in the optical regime of the pulsar X-ray and γ-ray spectra. The *Fermi*-LAT spectrum is described by a PL with photon index $\Gamma_\gamma = 1.04 \pm 0.07$ and an exponential cutoff at energy $E_{\rm cut} = 0.88 \pm 0.05$ GeV, yielding a flux $F_\gamma = (11.8 \pm 0.28) \times 10^{-11}$ erg cm^{-2} s^{-1} (Acero et al. 2015). The joint *XMM-Newton* and *Chandra* spectrum (Marelli et al. 2014) is described by a combination of a PL with photon index $\Gamma_{\rm X} = 2.68 \pm 0.04$ and a BB of temperature $k\,T = 0.060 \pm 0.0016$ keV, with a corresponding emitting area of radius $5.39^{+0.81}_{-0.71}$ km for a pulsar distance of 0.38 kpc. The spectral fit yields an $N_{\rm H} = (1.21 \pm 0.01) \times 10^{21}$ cm^{-2} and unabsorbed fluxes of $F_{\rm X}^{\rm PL} = (5.47 \pm 0.13) \times 10^{-13}$ and $F_{\rm X}^{\rm BB} = (7.63 \pm 0.19) \times 10^{-13}$ erg cm^{-2} s^{-1} for the PL and BB components, respectively. Similar spectral parameters were obtained by fitting the *Chandra* data alone with the same spectral model (Karpova et al. 2014; Auchettl et al. 2015). We computed the interstellar reddening along the line of sight, $E(B - V) \sim 0.22$, from the $N_{\rm H}$ and the relation of Predehl & Schmitt (1995). Then, we computed the unabsorbed spectral fluxes of the pulsar candidate counterpart in the $b_{\rm HIGH}$ and

[12] https://confluence.slac.stanford.edu/display/GLAMCOG/Public+List+of+LAT-Detected+Gamma-Ray+Pulsars

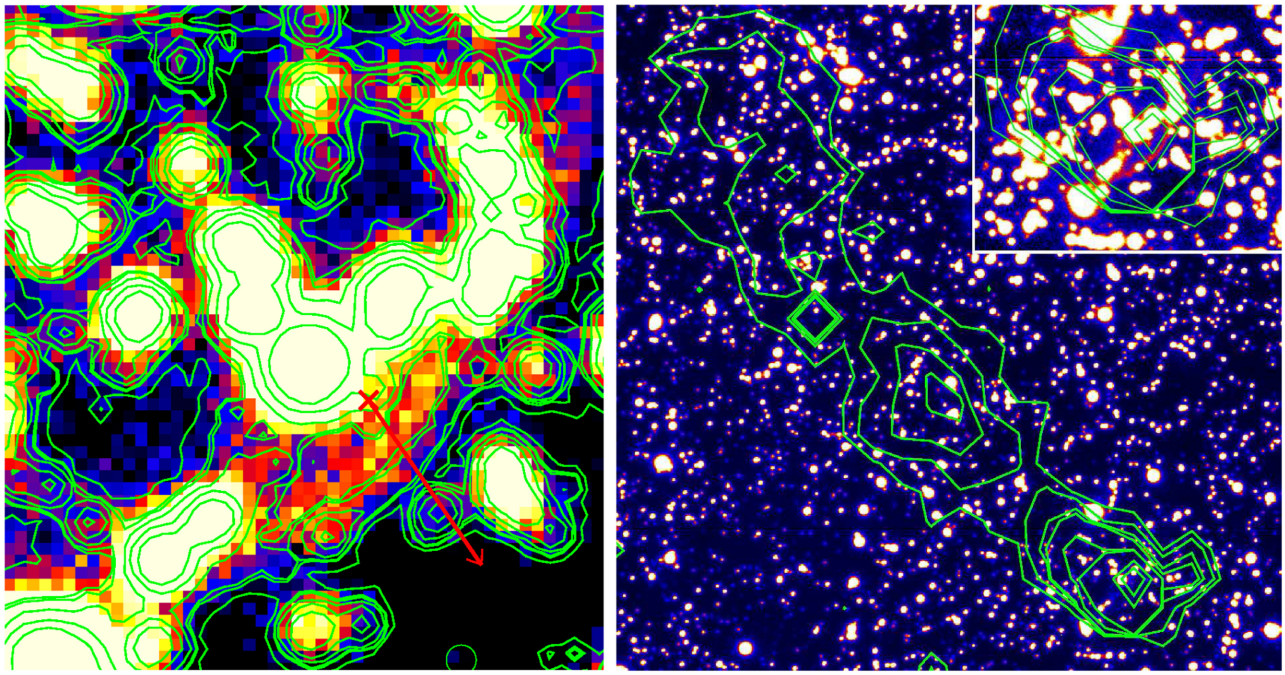

Figure 2. Left: NTT H_α image of the PSR J1741−2054 bow-shock nebula with the contours from the FORS2 b_{HIGH}-band image overlaid. The bow-shock displacement over the two epochs is apparent. The cross marks the pulsar position and the arrow its proper motion direction. Right: FORS2 image of the whole X-ray PWN region. The X-ray contours from the *Chandra* observation of PSR J1741−2054 are marked in green. The inset shows a close up view of the PWN around the pulsar position.

v_{HIGH} bands applying the interstellar extinction coefficients of Fitzpatrick (1999).

The b_{HIGH}- and v_{HIGH}-band optical fluxes lie well below the extrapolation of the X-ray PL, and above that of the γ-ray PL (Figure 3), suggesting that the non-thermal X-ray spectrum breaks at low energies. Single/multiple breaks in the multi-wavelength spectrum are observed in γ-ray pulsars, without an obvious relation to their characteristics, e.g., age and magnetic field (Mignani et al. 2016). More likely, they are related to different geometries of the emission regions in the pulsar magnetosphere and different viewing angles, which produce different light curve profiles. In the case of PSR J1741−2054, the break between the X-ray and γ-ray PLs indeed comes with a difference in the X/γ-ray light curves (Marelli et al. 2014).

Like in the X-rays, we expect that the optical emission of PSR J1741−2054 results from both the non-thermal emission from the neutron star magnetosphere and the thermal emission from the cooling neutron star surface as observed in other middle aged pulsars, i.e., PSR B0656+14, Geminga (Kargaltsev & Pavlov 2007), and PSR B1055−52 (Mignani et al. 2010). Indeed, the optical fluxes are above the extrapolation of the BB component to the X-ray spectrum and are not consistent with a Rayleigh–Jeans spectrum. This implies that any thermal component to the optical spectrum must be produced from a region on the neutron star surface presumably larger and colder than that producing the X-ray emission, and that a non-thermal PL component must be present. Obviously, with only two flux measurements, it is impossible to decouple these two components. Multi-band follow up observations are required for a spectral characterization.

The unabsorbed flux of the candidate counterpart is $F_{opt} \sim 4.09 \times 10^{-16}$ erg cm^{-2} s^{-1}, integrated over the v_{HIGH} band. This corresponds to a luminosity $L_{opt} \sim 7.06 \times 10^{27}$ erg s^{-1} for a distance of 0.38 kpc. The ratio to the pulsar rotational energy-loss rate yields an optical emission efficiency $L_{opt}/E_{rot} \sim 7.4 \times 10^{-7}$. We also compared the unabsorbed optical flux with the unabsorbed total X-ray flux F_X and the γ-ray flux F_γ. This yields $F_{opt}/F_X \sim 3.1 \times 10^{-4}$ and $F_{opt}/F_\gamma \sim 3.5 \times 10^{-6}$. All of these values are in the range of those computed for the other middle aged pulsars identified in the optical (see, e.g., Table 4 of Moran et al. 2013). This confirms that middle aged pulsars tend to have similar multi-wavelength emission properties.

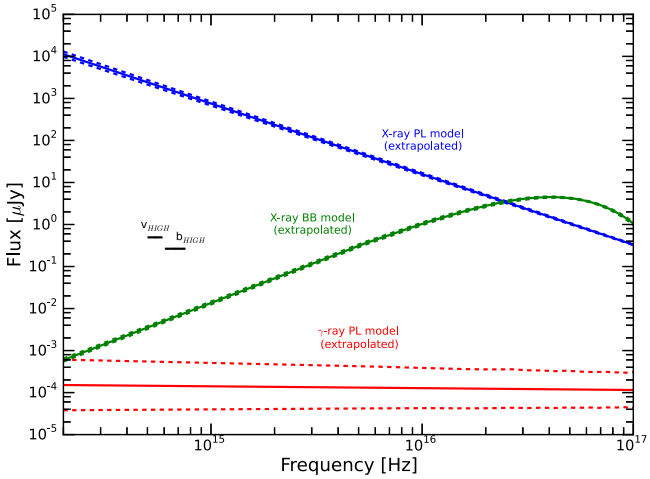

Figure 3. Spectral energy distribution of PSR J1741−2054. The optical flux measurements are labeled with the filter names. The blue and red lines represent the extrapolation in the optical regime of the PLs best-fitting the X and γ-ray spectra, respectively, whereas the green curve corresponds to the BB component to the X-ray spectrum. The dashed lines correspond to the 1σ error.

The better spatial resolution and sensitivity of our FORS2 images with respect to those of Romani et al. (2010) make it

possible to better resolve the morphology of the bow-shock nebula (Figure 2, left). Romani et al. (2010) noted that its shape is remarkably different with respect to the expectations of the model by Wilkin (1996), which assumes an isotropic pulsar wind. These authors computed the ratio of the perpendicular half-angular size of the nebula $\theta_{\perp}$ (measured through the pulsar) to the separation $\theta_{\parallel}$ between the pulsar and the apex of the nebula as a measure of the "flatness" of the bow-shock front and showed that the observed value can be reproduced by a model assuming an equatorially concentrated pulsar wind, aligned pulsar spin axis, and space velocity, and edge-on viewing geometry. Our images allow us to better constrain the distance of the bow-shock apex from the pulsar. Similar to what we did in Section 3, we extracted the nebula surface brightness profile along an image strip of $0\farcs625$ width, aligned with the pulsar proper motion direction (Auchettl et al. 2015), and we measured its position by fitting a simple Gaussian function. The resulting angular separation with respect to the proper-motion-corrected *Chandra* position of the pulsar (MJD 57156), $1\farcs6 \pm 0\farcs5$, is consistent with the value of $\sim 1\farcs5$ estimated by Romani et al. (2010) using the original *Chandra* position (MJD 55337) and the NTT H_{α} image (MJD 55063). A refined measurement of the pulsar proper motion, together with a more accurate pulsar localization from the identification of its optical counterpart, will allow us to probe in more detail the geometry of the momentum deposition by the pulsar particle wind.

The X-ray PWN is characterized by a segmented structure (Figure 2, right), with three bright emission lobes, one centered on the pulsar, and the other two almost aligned along the PWN tail, at $\sim 40''$ and $\sim 80''$ from the pulsar. The FORS2 images show that these two lobes cannot be produced by the combined emission of bright back/foreground stars and must be intrinsic to the PWN. In the case of a classical X-ray synchrotron emission, a variation of the mean interstellar density would cause the formation of such lobes, although this would imply a variation of a factor ~ 10 on a ~ 0.01 pc scale (for a 0.38 kpc distance). Alternatively, a spatial-dependent particle re-acceleration mechanism could be at work, as already invoked for other peculiar PWNe around, e.g., PSR J2055+2539 (Marelli et al. 2016) and PSR J1509−5850 (Klingler et al. 2016), or a different emission mechanism could be responsible for powering the X-ray PWN, like, e.g., in PSR J0357+3205 (Marelli et al. 2013).

5. CONCLUSIONS

Using the VLT, we found a possible candidate optical counterpart to PSR J1741−2054 ($m_b = 26.13$) based upon positional coincidence with its proper-motion-corrected *Chandra* coordinates. PSR J1741−2054 would then be the third γ-ray pulsar discovered by *Fermi* for which a candidate optical/infrared counterpart has been found, after PSR J0205+6449 (Moran et al. 2013) and PSR J1357−6429 (Zyuzin et al. 2016). Multi-epoch optical observations will allow us to measure the proper motion of the PSR J1741−2054 candidate counterpart and confirm the optical identification, whereas multi-band photometry will be needed to determine the pulsar spectrum in the optical. In the same VLT data, we also detected the bow-shock nebula around the pulsar and found that it is displaced to the southwest with respect to its position measured in the 2009 NTT data of Romani et al. (2010). The annual displacement (169^{+35}_{-54} mas yr^{-1}) is compatible with that expected for the pulsar proper motion, showing that the shock propagates in the ISM as the pulsar moves through it. Finally, we looked for extended optical emission associated with the X-ray PWN but we could not detect it down to a limit of ~ 28.1 magnitudes arcsec^{-2} in the $v_{\rm HIGH}$ band, the deepest obtained so far for this nebula.

We thank the anonymous referee for constructive comments to our manuscript. R.P.M. acknowledges financial support from the project TECHE.it. CRA 1.05.06.04.01 cap 1.05.08 for the project "Studio multilunghezze d'onda da stelle di neutroni con particolare riguardo alla emissione di altissima energia." The work of M.M. was supported by the ASI-INAF contract I/037/12/0, art.22 L.240/2010 for the project "Calibrazione ed Analisi del satellite NuSTAR."

Facility: Very Large Telescope.

REFERENCES

Abdo, A. A., Ackermann, M., Ajello, M., et al. 2009, Sci, 325, 840
Abdo, A. A., Ajello, M., Allafort, A., et al. 2013, ApJS, 298, 17
Acero, F., Ackermann, M., Ajello, M., et al. 2015, ApJS, 218, 23
Ackermann, M., Albert, A., Baldini, L., et al. 2015, Sci, 365, 801
Appenzeller, I., Fricke, K., Fürtig, W., et al. 1998, Msngr, 38, 9
Atwood, W. B., Abdo, A. A., Ackermann, M., et al. 2009, ApJ, 697, 1071
Auchettl, K., Slane, P., Romani, R. W., et al. 2015, ApJ, 802, 68
Brownsberger, S., & Romani, R. W. 2014, ApJ, 784, 154
Buzzoni, B., Delabre, B., Dekker, H., et al. 1984, Msngr, 94, 1
Camilo, F., Ray, P. S., Ransom, S. M., et al. 2009, ApJ, 705, 1
Caraveo, P. A., Bignami, G. F., Mereghetti, S., & Mombelli, M. 1992, ApJL, 395, L103
Chatterjee, S., & Cordes, J. M. 2002, ApJ, 575, 407
Cordes, J. M., & Lazio, T. J. W. 2002, arXiv:astro-ph/0207156
Fitzpatrick, E. L. 1999, PASP, 111, 63
Kargaltsev, O., & Pavlov, G. G. 2007, Ap&SS, 308, 287
Karpova, A., Danilenko, A., Shibanov, Y., Shternin, P., & Zyuzin, D. 2014, ApJ, 789, 97
Klingler, N., Kargaltsev, O., Rangelov, B., et al. 2016, ApJ, submitted, arXiv:1601.07174
Lasker, B. M., Lattanzi, M. G., McLean, B. J., et al. 2008, AJ, 136, 735
Manchester, R. N., Hobbs, G. B., Teoh, A., & Hobbs, M. 2005, AJ, 129, 1993
Marelli, M., Belfiore, A., Saz Parkinson, P., et al. 2014, ApJ, 790, 51
Marelli, M., De Luca, A., Salvetti, D., et al. 2013, ApJ, 765, 36
Marelli, M., Pizzocaro, D., De Luca, A., et al. 2016, ApJ, 819, 40
Mignani, R. P. 2011, ASpR, 47, 1281
Mignani, R. P., Pavlov, G. G., & Kargaltsev, O. 2010, ApJ, 720, 1635
Mignani, R. P., Rea, N., Testa, V., et al. 2016, MNRAS, submitted
Moran, P., Mignani, R. P., Collins, S., et al. 2013, MNRAS, 436, 401
Predehl, P., & Schmitt, J. H. M. M. 1995, A&A, 293, 889
Romani, R. W., Shaw, M. S., Camilo, F., Cotter, G., & Sivakoff, G. R. 2010, ApJ, 724, 908
Stetson, P. B. 1994, PASP, 106, 250
Wilkin, F. P. 1996, ApJL, 459, L31
Zyuzin, D., Zharikov, S., Shibanov, Y., et al. 2016, MNRAS, 455, 1746